35-GHz (Q-Band) Saturation Transfer Electron Paramagnetic Resonance Studies of Rotational Diffusion†

Michael E. Johnson* and James S. Hyde

ABSTRACT: The extension of saturation transfer electron paramagnetic resonance spectroscopy (ST-EPR) to an observational frequency of 35 GHz (Q band) is described. At this frequency the spectral resolution is greatly enhanced over that afforded at the 9.5-GHz (X-band) frequency used in most of the ST-EPR studies published to date. Thus, Q-band operation may provide an approach for the detailed analysis of the slow anisotropic motions believed to occur in many biomolecular systems. The spectral characteristics and the effects of various instrumental settings are described in detail for a model system of spin-labeled hemoglobin in water–glycerol solutions. Several spectral parameters are defined, and their potential use in monitoring various types of anisotropic motion is considered.

The application of spin-label rapid-passage saturation transfer EPR (ST-EPR)[1] to various biomolecular studies has shown a marked and continuing increase since its introduction by Hyde & Thomas (1973). Very recent applications include the use of several spin probes to study motional behavior within the hydrocarbon region of model membrane systems (Delmelle et al., 1980; Marsh, 1980), the use of a spin-label NAD^+ derivative to study lactate dehydrogenase solution conformation (Trommer & Gloggler, 1979), studies of spectrin interactions with the erythrocyte membrane (Fung et al., 1979; Lemaigre-Dubreuil et al., 1980), studies of F-actin rotational dynamics (Thomas et al., 1979), studies of the hydrodynamic properties of glyceraldehyde-3-phosphate dehydrogenase (Beth et al., 1979), studies of protein–protein interactions and rhodopsin rotational motion in membranes (Kusumi et al., 1978; Baroin et al., 1979; Davoust et al., 1980), and comparative studies of membrane fluidity for erythrocytes from normal and myotonic goats (Swift et al., 1980). Many of these and other applications have been discussed in recent reviews (Hyde, 1978; Hyde & Dalton, 1979; Hyde & Thomas, 1980).

From the studies published to date, two limitations in the use of ST-EPR techniques, as currently developed, are becoming apparent: (1) ST-EPR spectra in a variety of biomolecular systems provide qualitative evidence for the existence of anisotropic motion, but quantitative analysis of such motion is quite difficult due to spectral overlap of spin states and turning points,[2] and (2) approximately 0.1 mL of solution is required for the conventional X-band flat cell, limiting the types of studies that can be performed with some systems. The problem of anisotropic motion in ST-EPR has been approached experimentally through the use of spin probe–thiourea adduct (Gaffney, 1979) and lipid bilayer (Delmelle et al., 1980) model systems. Extensive theoretical calculations of ST-EPR spectral behavior have also been reported for the two cases where the diffusion tensor is either coincident with, or orthogonal to, the label magnetic tensor (Robinson & Dalton, 1980). However at X-band, with the commercially available ^{14}N spin-labels, the only clearly resolved spectral turning points are the low- ($m_I = +1$) and high-field ($m_I = -1$) z turning points. The x and y turning points for both of these spin states and all three turning points for the $m_I = 0$ spin state overlap in the center of the spectrum. Thus the amount of information about anisotropic motion obtainable from X-band spectra is limited.

As an approach to developing a more detailed understanding of anisotropic motion in the ST-EPR time domain, we report the extension of ST-EPR to an observational frequency of 35 GHz (Q band). At 35 GHz, spectral resolution is greatly enhanced due to increased g anisotropy; nearly all of the turning points for the three ^{14}N spin states are resolved. This paper describes in some detail the 35-GHz spectral characteristics and instrumental methods following the basic procedures outlined by Thomas et al. (1976) in their survey of X-band ST-EPR. In addition to increased spectral resolution, operation at 35 GHz provides the additional advantage that, for aqueous samples, the sample volume required is reduced from about 100–500 μL (for X-band) to approximately 2–5 μL. Future papers will describe applications to biomolecular systems exhibiting anisotropic motion.

Materials and Methods

Blood samples were obtained from the University of Illinois Hospital Blood Bank; hemoglobin was prepared from the pooled blood samples by the methods of Abraham et al. (1975) and kept under CO atmosphere until use. Mal-6 (Syva Corp.) spin-labeling of Hb followed previously published procedures (Johnson, 1978). Hb concentrations were determined from the visible absorption bands at 540 and 569 nm (Antonini & Brunori, 1971). Mal-6-labeled Hb was dissolved in various glycerol-water solutions to give a final Hb concentration of 30 mg/mL; glycerol–water ratios of the solutions were cor-

† From the Department of Medicinal Chemistry, University of Illinois at the Medical Center, Chicago, Illinois 60680 (M.E.J.), and the National Biomedical ESR Center, Department of Radiology, The Medical College of Wisconsin, Milwaukee, Wisconsin 53226 (J.S.H.). *Received October 14, 1980.* This work was supported in part by grants from the Research Corporation, the Chicago Heart Association, and the National Institutes of Health (HL-15168, HL-23697, GM-22923, GM-27665 and RR-01008). This work was done in part during the tenure of an Established Investigatorship from the American Heart Association (M.E.J.) and with funds contributed in part by the Chicago affiliate.

[1] Abbreviations used: EPR, electron paramagnetic resonance; ST-EPR, saturation transfer EPR; NAD^+, nicotinamide adenine dinucleotide; Mal-6, 4-maleimido-2,2,6,6-tetramethylpiperidin-1-yloxy; Hb, hemoglobin; PADS, peroxylaminedisulfonate.

[2] The term "turning point" is used to denote those points in the spectrum at which the angular rate of spectral diffusion goes to zero (i.e., $\partial H_R(\theta)/\partial(\cos\theta) = 0$, where $H_R(\theta)$ is the resonance field and θ is the angle between the nitroxide z axis and the external magnetic field). At these points rotational diffusion produces no spectral diffusion, and there is a buildup of spectral intensity in the out-of-phase displays. The turning points for a 35-GHz V_2' spectrum are shown in Figure 2. For further discussions of the physics giving rise to these displays, see Thomas et al. (1976) and Hyde & Dalton (1979).

0006-2960/81/0420-2875$01.25/0

rected for the Hb volume fraction (Jones et al., 1978). Viscosities of the glycerol–water solutions were measured with a Wells-Brookfield microviscometer. Rotational correlation times of the Mal-6-labeled Hb were calculated from the Stokes equation

$$\tau_R = 4\pi\eta r^3/(3kT) \quad (1)$$

where η is the solvent viscosity, r, the effective radius of the hydrated Hb molecule, is taken to be 30.5 Å (Jones et al., 1978), k is the Boltzmann constant, and T is the absolute temperature. Previous work has shown that, to a good approximation, the Mal-6 label is bound in a fixed orientation within its Hb binding site and exhibts little independent motion with respect to the Hb protein matrix (Johnson, 1978). Thus spectral behavior can be directly correlated with rates of Hb rotational motion.

Fully immobilized samples were prepared either by freezing concentrated (250 mg/mL) samples of Mal-6 labeled Hb at −12 °C or by precipitating 1:1 mixtures of unlabeled and Mal-6-labeled Hb with neutral saturated ammonium sulfate. The frozen Hb samples exhibited no change in spectral shape upon reducing the Hb concentration by a factor of 10; thus the high concentration was used to provide improved signal-to-noise ratios for the low-power and low-modulation spectra of Figures 5 and 6.

Samples were drawn into thin-wall glass capillary pipets with internal diameters ranging from 0.28 to 0.45 mm (depending on sample glycerol content and dielectric constant) which were then sealed at one end and inserted into a quartz tube (~2 mm i.d.) for placement in the EPR cavity. All samples were line samples, extending both above and below the active region of the cavity. Temperatures were monitored with a Fluke Model 2145A digital thermometer and a fine-wire copper–constantan thermocouple. The thermocouple junction was placed in the sample and positioned just above the active region of the cavity. Measurement accuracies are estimated to be approximately ±1 and ±1.5 °C above and below 0 °C, respectively. Temperatures were controlled with the standard Varian temperature-controller accessory.

EPR experiments were performed on a Varian E-9 spectrometer equipped with an E-110 35-GHz bridge containing an absorption/dispersion reference arm. The receiver module was modified as described by Thomas et al. (1976) to permit precise adjustment of the reference phase and to permit modulation at 50 kHz with second harmonic detection at 100 kHz. Spectra were accumulated in a Tracor-Northern NS-570A time averager and transmitted to a PDP 11/34 minicomputer for storage and later plotting.

Out-of-phase saturation transfer spectra were measured by use of a modified form of the self-null procedure (Thomas et al., 1976; deJager & Hemminga, 1978; B. J. Gaffney, unpublished data). In this procedure the field is centered on a major spectral line and the approximate phase null located by minimizing the signal. The exact phase null is then determined by progressively measuring the signal height at 1–2° steps above and below the approximate null; three or four measurements were generally made on each side of the approximate null. The signal amplitude was then plotted against the phase setting and a straight line drawn through the points, with the zero intercept being used as the final phase setting for the spectrum. Microwave power attenuation was generally set at 35 dB during nulling procedures. Increasing the attenuation by 5 dB did not change the null value significantly. We strongly emphasize the importance of using care in obtaining exact phase nulls. The ratios of out-of-phase signals to in-phase signals can be small, particularly for $\tau_R \simeq 10^{-7}$ s, and phase changes as small as 0.2° can produce measurable changes in spectral shape. (We also note that the modulation coil geometry at Q band in the Varian design can be expected to result in less phase inhomogeneity over the samples than the geometry at X band.)

Modulation amplitudes were set at 5.5 G for second harmonic absorption and 6 G for first harmonic dispersion ST-EPR measurements unless noted otherwise. Modulation amplitudes were determined by measuring the peak to peak separations of the downfield line of PADS at the appropriate modulation setting and adding either the full peak-to-peak first derivative line width (first harmonic absorption) or one-half the first derivative line width (second harmonic absorption) to the observed values (Robinson & Dalton, 1979).

Microwave power attenuations were set at 10.5 dB for second harmonic absorption (V_2'), and 7.5 dB for first harmonic dispersion (U_1') ST-EPR measurements unless noted otherwise. AT 10.5 dB the V_2' spectra exhibited approximately maximum intensity for intermediate correlation times. The value of 7.5 dB was chosen for U_1' measurements to maximize signal-to-noise ratios without producing excessive microwave heating. Klystron power output at the bridge was measured to be approximately 100 mW. Thus the power incident on the cavity was approximately 10 mW for V_2' and 20 mW for U_1' measurements. The effective microwave field at the sample will also depend on sample geometry; thus the CW saturation characteristics of PADS were measured. The "half-saturation point", $P_{1/2}$, for a dilute solution of PADS (1 mM in nitrogen-saturated D_2O, line sample) occurred at about 12-dB attenuation and can be used as a reference for comparing different sample geometries or spectrometers.

No special precautions were taken to exclude oxygen from the Hb solutions in this work. The spectra of samples which were CO saturated and sealed were compared with those of air-equilibrated samples and found to be essentially equivalent. However, for systems such as lipid bilayers, where oxygen solubility is higher, the oxygen-induced relaxation can induce significant changes in the ST-EPR spectra (C. Popp and J. S. Hyde, unpublished results). Thus for some systems it may be necessary either to exclude oxygen or to compensate for its effects on the ST-EPR displays.

Results and Discussion

Figure 1 shows the spectral behavior of the in-phase first harmonic absorption (V_1), second harmonic absorption (V_2), and first harmonic dispersion (U_1) and of the out-of-phase first harmonic absorption (V_1'), second harmonic absorption (V_2'), and first harmonic dispersion (U_1') signals for an immobilized Hb sample ($\tau_R = \infty$) and for one near the slow motion limit of conventional EPR ($\tau_R \simeq 8 \times 10^{-8}$ s). The in-phase spectra for all three displays show little change over the correlation time range from about 10^{-7} s up to complete immobilization. Likwise, the out-of-phase V_1' spectra appear relatively insensitive to motional changes over this correlation time range. The out-of-phase V_2' and U_1' spectra, however, appear quite sensitive to changes in rotational motion over this correlation time range. Considering first the V_2' display, we see that for τ_R near the conventional EPR "rigid limit" (~10^{-7} s), the spectral shape is qualitatively rather similar to the in-phase V_2 line shape. At the immobilization limit, however, the line shape is roughly what would be expected for an undifferentiated absorption (V_0) spectrum. The U_1' display shows a similar sensitivity to changes in rotational motion. At $\tau_R \simeq 10^{-7}$ s spectral intensity is exhibited only at the turning points; as rotational motion slows, intensity builds throughout the spectrum until it reaches the undifferentiated absorption-like

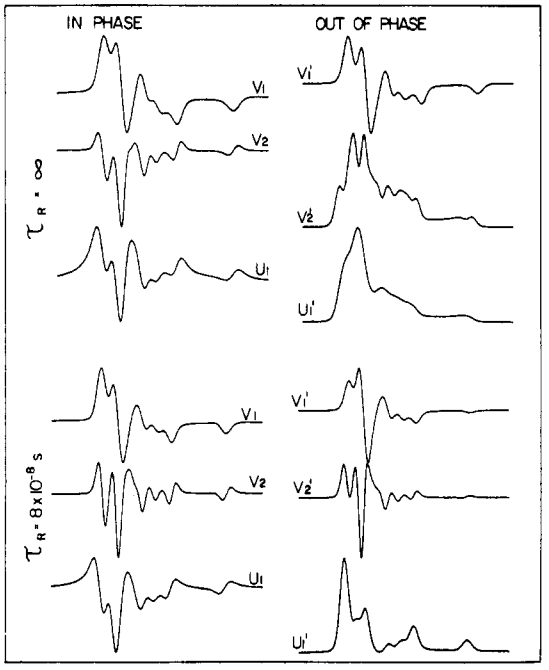

FIGURE 1: Experimental spectra illustrating the effects of slow rotational diffusion on 35-GHz EPR spectra obtained through various detection methods. The spectra in the top half are of Mal-6-labeled HbA (270 mg/mL) frozen at −12 °C. The spectra in the bottom half are of Mal-6-labeled HbA (270 mg/mL) in 0.05 M phosphate buffer at +3 °C. The spectra on the left were obtained with the reference phase of the phase-sensitive detector in phase with the Zeeman field modulation while those on the right were obtained with the reference 90° out of phase with the modulation. The detection frequency was 100 kHz; the peak-to-peak modulation amplitude, H_m, was 6 G for the first harmonic spectra and 5.5 G for the second harmonic spectra. Microwave power incident on the cavity was approximately 10 mW.

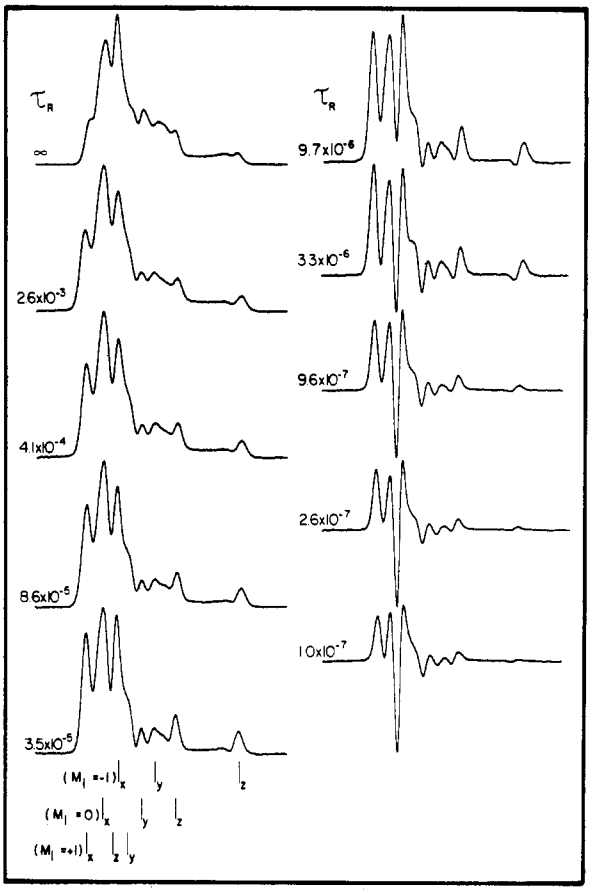

FIGURE 2: Second harmonic absorption saturation transfer spectra of Mal-6-labeled Hb. The spectrum at top left is of ammonium sulfate precipitated Hb. The other spectra are from Hb (30 mg/mL) in glycerol–water solutions at various temperatures and glycerol concentrations. Correlation times, τ_R, were calculated from the Stokes equation (eq 1) as discussed in the text. Spectrometer settings are given in the text. The x, y, and z turning points for the three nitrogen spin states are shown for the lower left spectrum. The increased g anisotropy at 35 GHz as compared to 9.5 GHz allows resolution of nearly all the turning points. [Compare with Figure 3 of Thomas et al. (1976).]

shape shown in the top half of Figure 1. Thus the basic behavior of the spectral displays is similar to that previously observed at X-band observational frequency (Thomas et al., 1976). The basic physical interpretation of the spectral displays has been previously discussed (Thomas et al., 1976; Hyde & Dalton, 1979) and will not be repeated here.

A V_2' spectrum with the three turning points (x, y, and z) for each of the three nitrogen nuclear spin states ($m_I = +1, 0, -1$) is shown at the lower left portion of Figure 2. Starting from the high-field side of the spectrum, the z turning points for spin states $m_I = -1, 0$ are clearly defined and well separated from other turning points; the y turning points for these spin states are also fairly well defined. From the low-field side of the spectrum the $x(+1, 0)$ turning points also appear well defined and reasonably separated from other turning points. Between these "end" regions of the spectrum, however, the $z(+1)$, $x(-1)$, and $y(+1)$ turning points appear to define an overlap region.

Figure 2 also contains representative V_2' spectra for correlation times from 1.0×10^{-7} s up to 2.6×10^{-3} s at approximately half order of magnitude intervals. The V_2' spectrum for an immobilized sample (precipitated Hb) is also shown. The spectra appear to exhibit the greatest overall sensitivity to motional rates over the range $10^{-6} \lesssim \tau_R \lesssim 10^{-4}$ s. However, the spectral regions appear to differ somewhat in their sensitivity to changes in motional rates. The downfield region is sensitive to τ_R changes down to about 10^{-7} s but appears to change little for $\tau_R > 10^{-4}$ s. The high-field region, on the other hand, changes little for $\tau_R \lesssim 10^{-6}$ s but shows sensitivity to τ_R out to at least 8×10^{-3} s.

The U_1' spectra shown in Figure 3 exhibit behavior qualitatively similar to that of the V_2' display. However the U_1' sensitivity to changes over the range $10^{-7} \lesssim \tau_R \lesssim 10^{-6}$ s appears to be significantly greater than that of the V_2' display, and the asymptotic "slow motion" limit appears to occur at around $\tau_R \simeq 10^{-4}$ s rather than the 10^{-3}–10^{-2} s limit observed for the V_2' display. Thus the dispersion ST-EPR display may offer an advantage for monitoring the shorter correlation times but will be of limited value for $\tau_R > 10^{-4}$ s (unless the modulation frequency is decreased).

In contrast to the situation at X band, the U_1' spectra can be obtained with signal-to-noise equivalent to those of the V_2' spectra in about the same amount of time. (In fact, it was usually much easier to obtain the phase null for the U_1' than for the V_2' display). However, for U_1' spectra from very weak samples, it was difficult to keep the AFC level high enough to maintain bridge stability without saturating the receiver. For both the V_2' and the U_1' displays, the out-of-phase signal intensity was about 10% of the in-phase signal intensity for $\tau_R \simeq 10^{-7}$ s. This increased to about 30% (V_2') and 90% (U_1') for $\tau_R = \infty$ (the precipitated sample). Absolute signal intensities for U_1' spectra are 5–10 times larger than those for V_2' spectra; the increased FM noise in dispersion, however, results in essentially equivalent signal-to-noise ratios for the two displays.

There are a variety of spectral intensity ratios that can be defined and used to monitor correlation times. Figure 4 characterizes those that we have found to be most reliable and

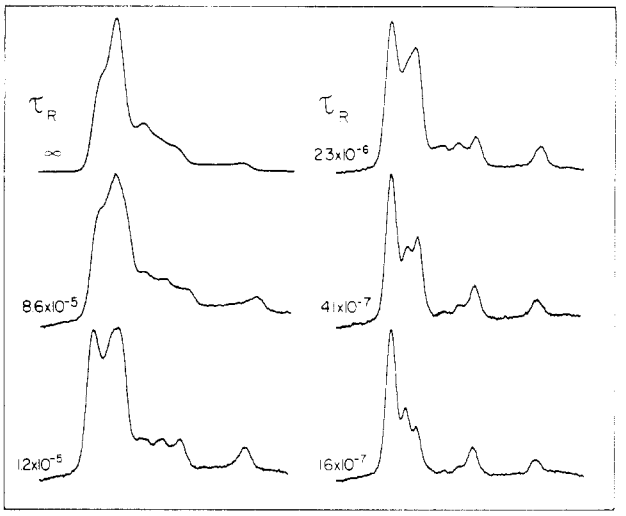

FIGURE 3: First harmonic dispersion saturation transfer spectra of Mal-6-labeled Hb. The spectrum at top left is of ammonium sulfate precipitated Hb. The other spectra are from Hb (30 mg/mL) in glycerol–water solutions at various temperatures and glycerol concentrations. Correlation times, τ_R, were calculated from the Stokes equation (eq 1) as discussed in the text. Spectrometer settings are given in the text. The slight base-line slope appears to be due to trace manganese in the wall of the glass capillaries.

consider to be most useful. In Figure 4a, the parameter E'/E is plotted, where E is the height of the peak at the high-field turning point, and E' is the height of the relatively flat region between the $z(-1)$ and $z(0)$ turning points at the position shown. This ratio will be primarily sensitive to the rate at which the nitroxide magnetic z axis rotates out of coincidence with the applied magnetic field and is thus effectively a monitor for motion about the nitroxide x and y axes. The spectra of Figure 2 suggest that the increase in this ratio for $\tau_R \lesssim 10^{-6}$ s is probably due to loss in resolution of the high-field turning point for short correlation times. This parameter should thus probably be considered useful only for $\tau_R \lesssim 5 \times 10^{-6}$ s; it exhibits continued sensitivity out to the longest correlation times measured.

The ratio D'/D, plotted in Figure 4b, was measured as shown in the inset spectrum. This ratio is also essentially a measure of z axis motional rates and, due to its monotonic behavior and greater signal intensities, will be preferable to the E'/E ratio over the full correlation time range. For highly anisotropic rotation the two parameters may exhibit a moderate discrepancy depending on the relative orientations of the magnetic and diffusional principal axes (M. Johnson, unpublished observations).

The parameter C'/C, plotted in Figure 4c, is quite sensitive to changes in rotational motion over the range $10^{-7} \lesssim \tau_R \lesssim 10^{-4}$ s but is essentially constant for longer correlation times. The trough at C' is between the x and y turning points for both $m_I = 0$ and $m_I = -1$ spin states. Thus the ratio C'/C should be sensitive to x–y averaging and may be sensitive to x–z averaging. It should not be sensitive to y–z averaging (provided the turning points are stationary).

Figure 4d shows the behavior of the ratio B'/B, with B' and B measured as shown on the inset spectrum. This ratio is most sensitive to correlation time changes over the faily restricted range of $10^{-7} \lesssim \tau_R \lesssim 10^{-5}$ s and reaches an essentially constant value for $\tau_R \gtrsim 4 \times 10^{-5}$ s. From Figure 2, the $z(+1)$ turning point should be located approximately at the position of the dip, B′. Intensity at the turning point should be relatively constant; thus loss of z-axis correlation with the magnetic field should have little effect on this ratio. The peak at B appears to correspond to the $x(0)$ turning point, and the dip, B′, lies

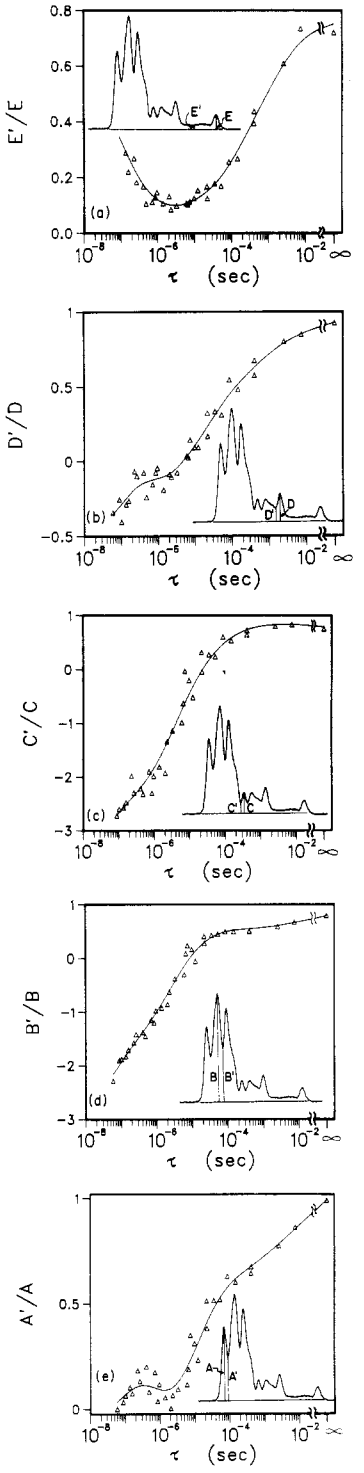

FIGURE 4: Dependence on τ_R of the various spectral parameters derived from the V_2' spectra (see Figure 2). The points at finite correlation times are from the Hb–glycerol experiments. The point labeled ∞ is from ammonium sulfate precipitated Hb.

between it and the $y(0)$ and $z(0)$ turning points. It is also located approximately midway between the $x(+1)$ and $y(+1)$ turning points. Thus it should be particularly sensitive to x–y averaging and may be affected by x–y averaging, but should not be sensitive to y–z averaging. Preliminary model membrane studies confirm the sensitivity to x–y averaging (M. Johnson, unpublished results).

The ratio A'/A, shown in Figure 4e, exhibits good sensitivity to changes in rotational motion from $\tau_R \simeq 10^{-5}$ s up to the longest correlation times measured. For $\tau_R < 10^{-5}$ s, the ratio fluctuates in value between 0 and 0.2, and is not considered

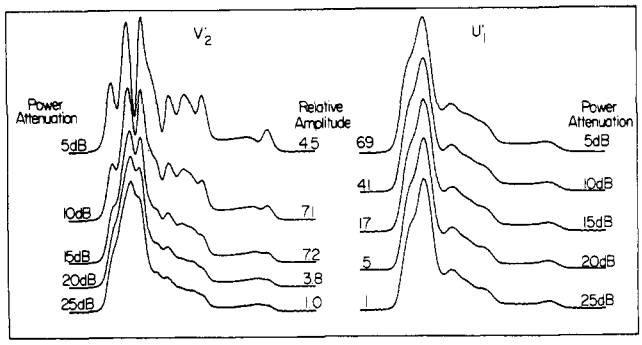

FIGURE 5: Microwave power dependence of saturation transfer spectra obtained from Mal-6-labeled HbA frozen at −12 °C. Relative amplitudes are referenced to the spectra at 25-dB attenuation. Modulation amplitudes were 5.5 (V_2') and 6 G (U_1').

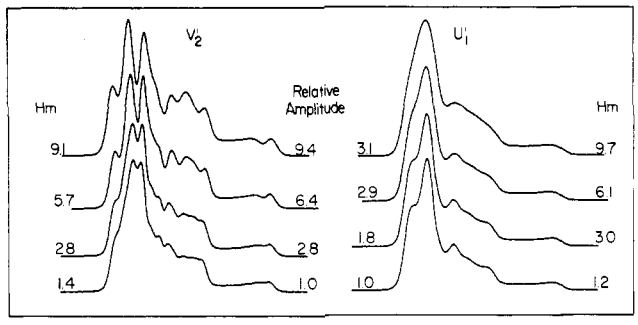

FIGURE 6: Modulation amplitude dependence of saturation transfer spectra obtained from Mal-6-labeled HbA frozen at −12 °C. Relative spectral amplitudes are referenced to the spectra at the lowest modulations. Microwave attenuation was set at 10 dB.

to be reliable. This ratio will be primarily sensitive to the rate at which the nitroxide magnetic x axis rotates out of coincidence with the magnetic field and is thus effectively a monitor for diffusion of the nitroxide about the y and z axes.

Several other spectral ratios have also been defined and examined. However, of the possibilities available, the parameters defined by Figure 4a–e appear to be the best behaved and most amenable to interpretation. The five parameters defined here should provide a substantial improvement (compared to X band) in defining the relative orientations of magnetic and diffusional axes when the system is undergoing anisotropic rotational diffusion. The parameters E'/E and D'/D both describe loss of z-axis correlation with the external magnetic field, A'/A describes loss of x-axis correlation, B'/B probably describes primarily loss of x-axis correlation, and C'/C probably reflects most strongly loss of y-axis correlation with the magnetic field. (We recognize that there is a certain imprecision in these preceding statements. It is not clear whether ST-EPR measures rotational diffusion or loss of correlation, nor is it clear how to relate diffusion constants and correlation times unless the form of the potential in which anisotropic diffusion occurs is known. These questions require further theoretical analysis.)

It should be strongly emphasized that use of the parameters and plots defined above is valid *only* if all of the spectral turning points are essentially stationary. This limitation will be a particularly important consideration for systems in which fast averaging occurs about one of the nitroxide magnetic axes. Under these conditions only the turning points for the diffusional symmetry axis will be stationary. The nonstationary turning points undergoing averaging will vary in intensity, position, and resolution as τ_R changes. The spectral parameters defined above (and by Thomas et al. (1976) for X-band studies) can no longer be properly interpreted under these circumstances. This problem has been encountered by Delmelle et al. (1980) in a ST-EPR study of dipalmitoylphosphatidylcholine multilayers with intercalated cholestane spin probe, but the limitations in the use of the spectral ratios were not fully discussed.

This is not to imply that ST-EPR cannot be used to analyze systems simultaneously undergoing both fast and very slow motions. However, such an analysis will require the use of both conventional and ST-EPR displays and will require further analysis of the mechanisms giving rise to ST-EPR spectral intensity in the presence of partial fast averaging.

The effects of microwave power on the V_2' and U_1' spectra of frozen Mal-6-labeled Hb are shown in Figure 5. The U_1' display is essentially independent of microwave power. The V_2' spectra are strongly affected at an attenuation of 5 dB, moderately affected at 10 dB, and are nearly constant in line shape from 15 to 25 dB. The maximum V_2' intensity is observed at an attenuation of approximately 12 dB. This behavior is qualitatively similar to that observed at X band (Thomas et al., 1976).

Figure 6 indicates that the V_2' and U_1' line shapes are both affected by modulation amplitude, with the V_2' line shape showing the greater effects. Both displays appear to exhibit nearly constant line shapes for modulations of 3 G or less. This behavior is again similar to that observed at X band (Thomas et al., 1976).

The instrumental settings used in this study represent a compromise between maximizing signal intensity and minimizing spectral sensitivity to instrumental settings. Under these conditions the accumulation times for the V_2' Hb–glycerol spectra of Figure 3 ranged from about 20 to 60 min at a spin-label concentration of about 0.9 mM. The low concentration limit which appears to be practical at these instrumental settings is around 0.1–0.3 mM in label, depending somewhat on τ_R and dielectric constant. (The principal limitation at low concentration, in fact, is difficulty in accurately determining the phase null, rather than in obtaining spectra with adequate signal-to-noise ratio.) This low concentration limit is about an order of magnitude higher than that reported by Hyde (1978) at X band ($\sim 2 \times 10^{-5}$ M). From previous EPR measurements, a factor of 2 difference would normally be expected with capillaries at both frequencies. The additional factor of 5 probably arises primarily from the larger volume capacity of the flat-cell geometry used to determine sensitivity limits at X band.

In summary, the present study demonstrates the potential utility of 35-GHz ST-EPR for biomolecular systems exhibiting complex motional behavior in the slow-motion time regime. The ST-EPR spectral characteristics at Q band are qualitatively similar to those at X band but should offer increased resolution for motions which preferentially affect specific nitroxide magnetic axes. The V_2' high-field spectral parameters also appear sensitive to correlation times about 5–10 times longer than the 10^{-3} s slow motion limit of the X-band V_2' ST-EPR display. Specific applications of these techniques to biomolecular systems will be described in future communications.

Acknowledgments

We thank Dr. Peter Gutierrez for his help with the equipment in the early phases of this work and Dr. Christopher Felix for the development of computer programs used in storing and plotting spectra.

References

Abraham, E. C., Walker, D., Gravely, M., & Huisman, T. H. J. (1975) *Biochem. Med. 13*, 56–77.

Antonini, E., & Brunori, M. (1971) *Hemoglobin and Myoglobin in Their Reactions with Ligands*, North-Holland, Amsterdam.
Baroin, A., Bienvenue, A., & Devaux, P. F. (1979) *Biochemistry 18*, 1151–1155.
Beth, A. H., Wilder, R., Wilkerson, L. S., Perkins, R. C., Merriwether, B. P., Dalton, L. R., Park, C. R., & Park, J. H. (1979) *J. Chem. Phys. 71*, 2074–2082.
Davoust, J., Bienvenue, A., Fellman, P., & Devaux, P. F. (1980) *Biochim. Biophys. Acta 596*, 28–42.
deJager, P. A., & Hemminga, M. A. (1978) *J. Magn. Reson. 31*, 491–496.
Delmelle, M., Butler, K. W., & Smith, I. C. P. (1980) *Biochemistry 19*, 698–704.
Fung, L. W.-M., Soo Hoo, M. J., & Meena, W. A. (1979) *FEBS Lett. 105*, 379–383.
Gaffney, B. J. (1979) *J. Phys. Chem. 83*, 3345–3349.
Hyde, J. S. (1978) *Methods Enzymol. 49*, 480–511.
Hyde, J. S., & Thomas, D. D. (1973) *Ann. N.Y. Acad. Sci. 222*, 680–692.
Hyde, J. S., & Dalton, L. R. (1979) in *Spin Labeling; Theory and Applications* (Berliner, L. J., Ed.) Vol. 2, pp 1–70, Academic Press, New York.
Hyde, J. S., & Thomas, D. D. (1980) *Annu. Rev. Phys. Chem. 31*, 293–317.
Johnson, M. E. (1978) *Biochemistry 17*, 1223–1228.
Jones, C. R., Johnson, C. S., & Penniston, J. T. (1978) *Biopolymers 17*, 1581–1593.
Kusumi, A., Ohnishi, S., Ito, T., & Yoshizawa, T. (1978) *Biochim. Biophys. Acta 507*, 539–543.
Lemaigre-Dubreuil, Y., Henry, Y., & Cassoly, R. (1980) *FEBS Lett. 113*, 231–234.
Marsh, D. (1980) *Biochemistry 19*, 1632–1637.
Robinson, B. H., & Dalton, L. R. (1979) *Chem. Phys. 36*, 207–237.
Robinson, B. H., & Dalton, L. R. (1980) *J. Chem. Phys. 72*, 1312–1324.
Swift, L. L., Atkinson, J. B., Perkins, R. C., Dalton, L. R., & LeQuire, V. S. (1980) *J. Membr. Biol. 52*, 165–172.
Thomas, D. D., Dalton, L. R., & Hyde, J. S. (1976) *J. Chem. Phys. 65*, 3006–3024.
Thomas, D. D., Seidel, J. L., & Gergely, J. (1979) *J. Mol. Biol. 132*, 257–273.
Trommer, W. E., & Glöggler, K. (1979) *Biochim. Biophys. Acta 571*, 186–194.

Laser Chemically Induced Dynamic Nuclear Polarization Study of the Reaction between Photoexcited Flavins and Tryptophan Derivatives at 360 MHz†

Elizabeth F. McCord, Rodney R. Bucks, and Steven G. Boxer*

ABSTRACT: Chemically induced dynamic nuclear polarization (CIDNP) is generated when tryptophan (Trp), its derivatives, or Trp-containing peptides react with photoexcited flavins in a 360-MHz NMR spectrometer. In contrast to tyrosine (Tyr), we find that the nuclear polarization of Trp originates in an electron-transfer reaction. By use of a series of Trp derivatives, the unpaired spin-density distribution of the Trp radical cation and the ground-state NMR spectrum of Trp are analyzed in detail. The signs and the relative magnitudes of the proton isotropic hyperfine coupling constants for each position around the indole ring in the radical cation deduced from these measurements are the following: position $3 \gg 2 \sim 4 \sim 6 > 1 \gg 5 > 7$, with positions 1, 2, 3, 4, and 6 positive, 5 negative, and 7 essentially zero. This result is inconsistent with most available calculations of the unpaired spin-density distribution but is compatible with the pattern of electrophilic aromatic substitution. The origin of this discrepancy is discussed in detail. Possible mechanistic complications in the reaction leading to CIDNP are discussed. The laser CIDNP spectra of the Trp-rich peptides gramicidins A and B are presented as examples of the resolution enhancement obtained with this technique.

The photophysics and photochemistry of both tryptophan (Trp)[1] and flavins have been studied extensively and exploited to probe their environment and reactivity in a large number of proteins. Trp is a very useful reporter because it can be selectively excited, and its fluorescence emission provides a probe of local conformational flexibility (Munro et al., 1979) or dielectric properties in the protein (Donovan, 1969). It is ideally suited for structural studies in proteins using resonant energy transfer to or from other residues or prosthetic groups (Stryer & Haugland, 1967; Yguerabide et al., 1970). Recently, the properties of the Trp triplet state have been used

† From the Department of Chemistry, Stanford University, Stanford, California 94305. *Received October 30, 1980.* This research was supported by the Research Corporation and National Institutes of Health Grant GM 27738. The 360-MHz NMR spectra were obtained at the Stanford Magnetic Resonance Laboratory supported by National Science Foundation and National Institutes of Health Grants GR 23633 and RR 00711, respectively. E.F.M. is the recipient of a National Science Foundation Predoctoral Fellowship, and S.G.B. is an Alfred P. Sloan and Camille and Henry Dreyfus Teacher-Scholar Fellow.

[1] Abbreviations used: CI, configuration interaction; CIDNP, chemically induced dynamic nuclear polarization; COT, cyclooctatetraene; Me_2SO, dimethyl sulfoxide; ESR, electron spin resonance; His, histidine; HMO, Huckel molecular orbital; HOMO, highest occupied molecular orbital; INDO, intermediate neglect of differential overlap; LCAO, linear combination of atomic orbitals; LUMO, lowest unoccupied molecular orbital; MO, molecular orbital; NMR, nuclear magnetic resonance; Phe, phenylalanine; SCE, standard calomel electrode; SCF, self-consistent field; TBAP, tetra-*n*-butylammonium perchlorate; Me_4Si, tetramethylsilane; Trp, tryptophan; Tyr, tyrosine.

0006-2960/81/0420-2880$01.25/0